Emad M. M. Ewais, Amira M. M. Amin, Yasser M. Z. Ahmed, Eman A. Ashor, Ulrike Hess, Kurosch Rezwan

Combined effect of magnesia and zirconia on the bioactivity of calcium silicate ceramics at C \S ratio less than unity

Journal Article as: peer-reviewed accepted version (Postprint)

DOI of this document*(secondary publication): 10.26092/elib/2622

Publication date of this document: 03/11/2023

* for better findability or for reliable citation

Recommended Citation (primary publication/Version of Record) incl. DOI:

Emad M.M. Ewais, Amira M.M. Amin, Yasser M.Z. Ahmed, Eman A. Ashor, Ulrike Hess, Kurosch Rezwan,
Combined effect of magnesia and zirconia on the bioactivity of calcium silicate ceramics at C\S ratio less than unity,
Materials Science and Engineering: C, Volume 70, Part 1, 2017, Pages 155-160, ISSN 0928-4931,
https://doi.org/10.1016/j.msec.2016.08.057

Combined effect of magnesia and zirconia on the bioactivity of calcium silicate ceramics at C\S ratio less than unity

Emad M.M. Ewais [a,*], Amira M.M. Amin [a], Yasser M.Z. Ahmed [a], Eman A. Ashor [b], Ulrike Hess [c], Kurosch Rezwan [c]

[a] Refractory & Ceramic Materials Division (RCMD), Advanced Materials Department, Central Metallurgical R&D Institute (CMRDI), P.O. Box 87, Helwan, 11421, Cairo, Egypt
[b] Chemical Engineering Department, Faculty of Engineering, El-Minia University, El-Minia, Egypt
[c] Advanced Ceramics, University of Bremen, Am Biologischen Garten 2, 28359 Bremen, Germany

Keywords:
Calcia-silica
Magnesia
Zirconia
SBF
Bioactivity
Vickers hardness
Fracture toughness

A B S T R A C T

This paper describes the effect of magnesia in the presence of zirconia on the bioactivity, microstructure and physico-mechanical properties of calcium silicate composition adjusted at calcia/silica ratio(C/S) of 0.5. A mixture from calcium carbonate and silica was conducted at C/S of 0.5. 20 wt.% of magnesia and 5-25 wt.% of ZrO_2 were added. Each mixture was mixed with ethanol in a planetary ball mill, dried, formed and fired at a temperature of 1325 ± 5 °C. Phase composition, FE-SEM, and physico-mechanical properties of the fired specimens were determined and explained. The in vitro bioactivities of these specimens were investigated by analysis of their abilities to form apatite in the simulated body fluid (SBF) for a short time (7 days) using SEM-EDS. The findings indicated that the surface of the specimens containing 5 and 15 wt.% ZrO_2 were completely covered by single and multilayered hydroxyapatite (HA) precipitate typical to "cauliflower" morphology, respectively. The surface of the specimen containing 25 wt.% ZrO_2 did not cover, but there are some scattered HA precipitate. The differences among the results were rationalized based on the phase composition. Vickers hardness and fracture toughness of the specimens of highly promised bioactivity were 2.32–2.57 GPa and 1.80–1.50 MPa. $m^{1/2}$, respectively. The properties of these specimens are similar to the properties of human cortical bone. Consequently, these composites might be used as bone implant materials.

1. Introduction

Bioceramics have become an important class of biomaterials in particular bioactive ceramics which directly form chemical bonds with bone tissues. The oldest bioactive material is the glass 45S5 (bioglass) which was first proposed by Hench et al. [1]. The CaO-SiO_2 based ceramics have been regarded as potential candidates for artificial bone due to their excellent bone bioactivity and biocompatibility. However, they cannot be used as implants under a heavy load because of their poor of the mechanical properties, in particular fracture toughness [2, 3]. Thus, the bioceramic materials with high mechanical properties as well as high apatite mineralization have become the bottleneck. Many researchers devoted their efforts to overcome this shortcoming. Magnesia (MgO) was added to CaO-SiO_2 ceramics and the results recorded gave a remarkable improvement in their mechanical properties through the formation of new phases such as akermanite ($Ca_2MgSi_2O_7$) and diopside, ($CaMgSi_2O_6$) [4–9]. However, the developed phases have high mechanical properties, but they have a low apatite formation in SBF compared with calcium silicate ceramics [6]. Other researchers have tried to find new applications that meet these requirements. High strength inert zirconia or metal substrate coating by wollastonite, hydroxyapatite and bioactive glass were proposed to match such purpose [3] [10–15]. On the other hand, zirconia ceramics have attractive properties such as high strength and fracture toughness for biomedical applications [16]. They have been applied in the heads of hip joint prostheses. However, Zirconia does not bond to the living bone. Interestingly, in 2001, Kokubo et al. pointed that zirconia ceramics exhibit a bone bonding ability from apatite formation when their surfaces are functionalized by hydroxyl(−OH) groups [17]. A nano-composite of ceria- stabilized tetragonal zirconia polycrystals (Ce-TZP) and alumina (Al_2O_3) polycrystals induced apatite forming ability via chemical treatments in aqueous solutions of H_3PO_4, H_2SO_4, HCl or NaOH [18]. Thus, the addition of zirconia may improve the biological and mechanical properties together. In this work, additional efforts were added to solve this problem through a systematic study. Designing new specimens containing calcia, magnesia and silica with different additions of zirconia were examined. Physico-mechanical properties and apatite forming ability have been determined. These specimens were constructed to take advantage of the combination of both bioactive phases (diopside, akermanite) and bioinert phase (baddeleyite). The results were compared with the reported data.

* Corresponding author.
E-mail address: dr_ewais@hotmail.com (E.M.M. Ewais).

Table 1
Chemical composition analysis of silica and zirconia as measured by XRF.

Oxides	Chemical composition, Wt%	
	Silica	Zirconia
ZrO_2	–	98.32
SiO_2	97.93	0.75
Al_2O_3	0.85	0.30
Na_2O	0.10	0.13
MgO	0.08	–
P_2O_5	–	0.06
SO_3	–	–
K_2O	0.10	–
CaO	0.84	0.16
TiO_2	0.10	0.11
Fe_2O_3	–	0.12
F	–	–
Cl	–	0.05
L.O.I.	–	–

2. Materials and experimental procedure

2.1. Materials

Most of the raw materials utilized in this investigation were chemically grade materials. $CaCO_3$ as a source of calcia (C: CaO) (Fisher Chemical, UK), magnesia (M: MgO) (LOBA Chemie for laboratory reagents and fine chemicals, India), zirconia (Z: ZrO_2) (SEPR, France) and quartz as a source of silica (S: SiO_2) (El-Nasr Company for Refractories and Ceramics "Sornaga", Egypt) were used. The chemical analysis of zirconia and silica powders supported by analytical XRF (Model advanced axios Netherlands) was given in Table 1. MgO was a heavy extra powder of purity of 99% and its particle size was <5 μm. The particle size of zirconia and silica was given in Table 2. The particle size distribution of zirconia and silica was measured using a laser light-scattering particle-size analyzer (Model LB500, Horiba. Tokyo).

2.2. Experimental procedure

A mixture of calcium carbonate and silica was conducted at C/S molar ratio of 0.5. 20 wt.% of magnesia and 5–25 wt.% of ZrO_2 were added. The mixtures composition was given in Table 3. The mixtures were wet mixed with ethanol in a planetary mill for 45 min using a zirconia ball to produce a homogenous mixture. The mixtures were dried and ground to pass through a 0.1 mm sieve. The powders were uni-axially pressed (KPD-30 A, Spain) at 60 MPa into a cylindrical shape of 2.3 cm diameter and 1 cm length. The specimens were dried in oven at 110 °C for 24 h and then fired at 1325 ± 5 °C for 2 h in a programmable electric furnace (HT 16/17, Nabertherm, Germany). The temperature of the specimens was raised from room temperature to the targeted firing temperature with a constant rate of 4 °C/min.

2.3. Characterization

Phase composition and crystalline phases in sintered specimens were identified by advanced X-ray powder diffraction using Bruker advanced X-ray diffractometer model D8 Kristalloflex (Ni-filtered Cu Kα radiation; λ = 1.544 Å, Germany). In addition, the Crystallite sizes were calculated from the XRD pattern by applying Scherrer's equation.

Table 2
Particle size distribution of silica and zirconia powders.

Material	Particle size, μm		
	d_{10}	d_{50}	d_{90}
Silica	2.69	25.95	104.70
Zirconia	1.32	5.38	13.95

Table 3
Compositions of A, B, C and D composites.

Mixture	Composition, wt.%			
	SiO_2	$CaCO_3$	MgO	ZrO_2
A	42.16	37.80	20.00	0.00
B	40.05	35.90	19.00	5.00
C	35.84	32.13	17.00	15.00
D	31.62	28.35	15.00	25.00

Table 4
Ion concentrations of SBF and human blood plasma (mM).

	Na^+	K^+	Mg^{2+}	Ca^{2+}	Cl^-	HCO_3^-	HPO_4^{2-}
SBF	142.00	5.00	1.50	2.50	148.80	4.20	1.00
Blood Plasma	142.00	5.00	1.50	2.50	103.00	27.00	1.00

Microstructural features of the sintered specimens were characterized using a field emission scanning electron microscope (FESEM; QUANTA FEG250 Made in NL). The surfaces of the specimens were examined using backscattered electron signals (BSE). Elemental analysis of each phase was also performed using the energy dispersive X-ray spectroscopy (EDX) equipped in the FESEM.

The apatite-formation ability of the obtained sintered specimens were evaluated by soaking in a simulated body fluid (SBF) solution at pH 7.45 and temperature of 36.5 °C for 7 days. The SBF solution was prepared according to the procedure described by Kokubo and Takadama [19]. Its ion concentrations were similar to those in human blood plasma as shown in Table 4. After soaking for 7 days, the specimens were rinsed with water, dried at ambient conditions and characterized by SEM.

Apparent porosity and bulk density of sintered specimens were determined by an Archimedes immersion technique using kerosene [20].

Vickers hardness (H_V) and fracture toughness (K_{IC}) of the obtained ceramic specimens were determined at room temperature on the polished surface considering an average of five indentations using a Vickers indentation method [21–25] with 20 kg load for 15 s. Vickers hardness was computed using the following relation:

$$Hv = 0.0018544\left(p/d^2\right)$$

where p is the indentation load (N), d is an average length of the two

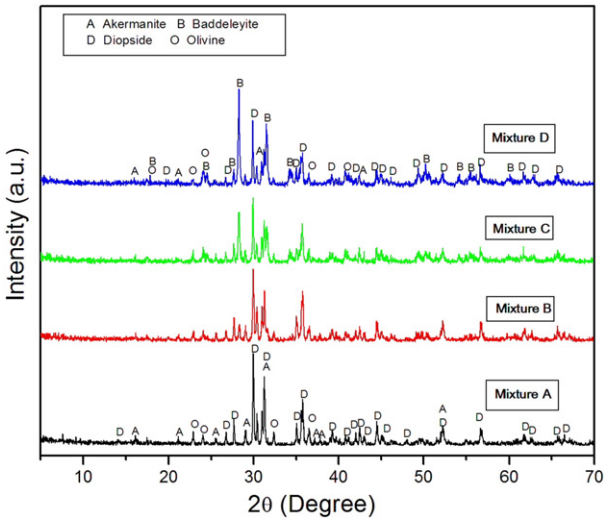

Fig. 1. X ray patterns of the sintered A, B, C and D specimens.

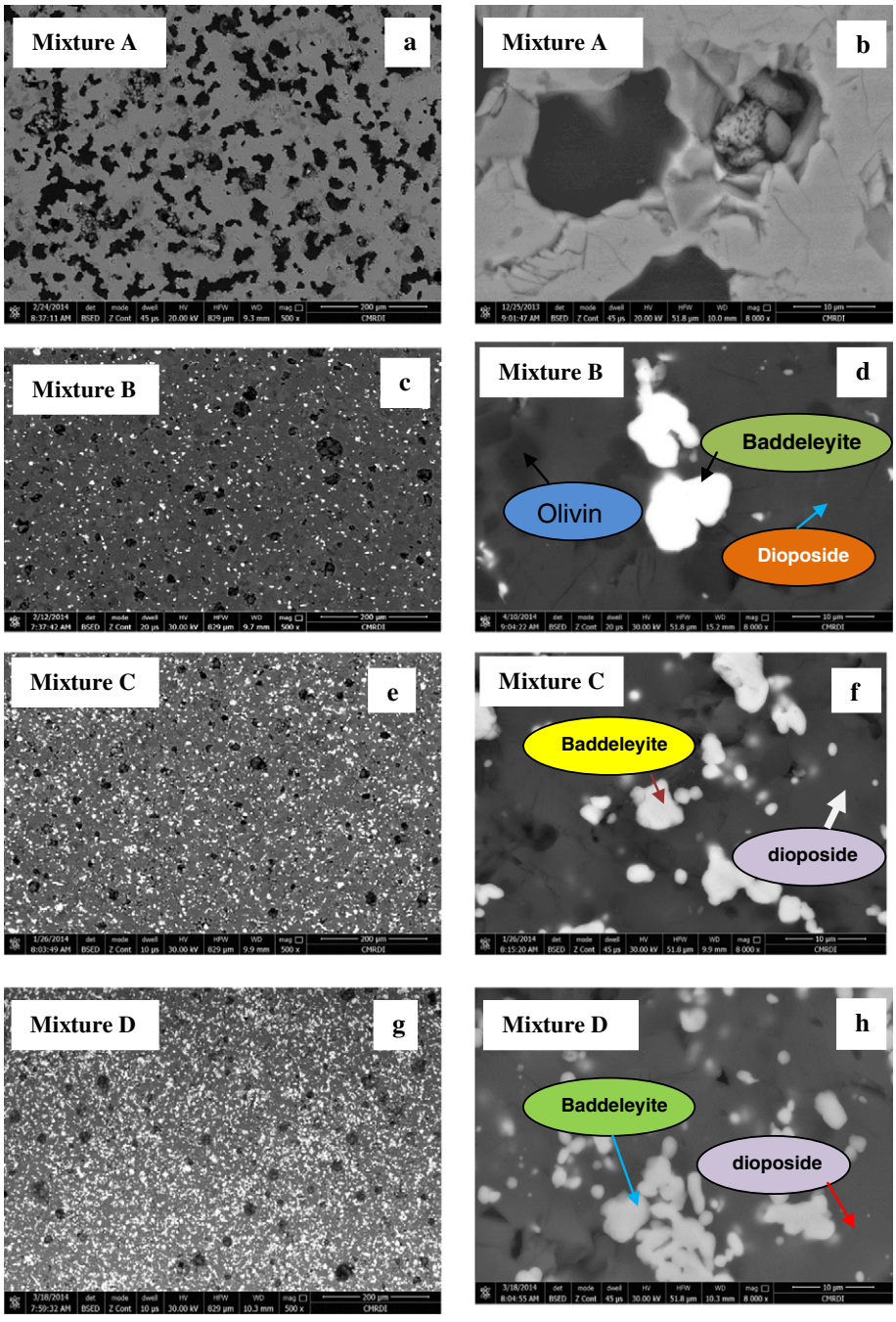

Fig. 2. FESEM micrographs of the sintered A, B, C and D specimens.

diagonals of the indentation, (mm) and Hv is the Vickers hardness in the unit of (GPa).

On the other hand, the fracture toughness was calculated through applying one of the following formulas based on the crack type [26–28].

$K_{IC} = 0.0515\ p/c^{3/2}$ for Palmqvist shaped-crack

$K_{IC} = 0.0726\ p/c^{3/2}$ for half-penny shaped-crack

where c is the crack length measured from the middle of the Vickers indentation (m), p is the indentation load (N) and K_{IC} is the fracture toughness ($MPa \cdot m^{1/2}$).

Table 5
Physical properties of the sintered A, B, C and D specimens.

Mixture	Bulk density, g/cm^3	Apparent porosity, %	Linear shrinkage, %
A	2.90 ± 0.02	3.50 ± 0.10	16.52 ± 0.02
B	3.04 ± 0.01	2.30 ± 0.01	17.17 ± 0.01
C	3.20 ± 0.01	2.30 ± 0.01	17.60 ± 0.01
D	3.38 ± 0.01	2.96 ± 0.02	19.78 ± 0. 12

Table 6
Vickers hardness of the sintered A, B, C, and D specimens.

Mixture	Hardness, GPa
A	1.88 ± 0.06
B	2.32 ± 0.03
C	2.57 ± 0.02
D	2.25 ± 0.00

Table 7
Crack pattern resulted from indentation fracture at 20 kg of the sintered A, B, C and D specimens.

Mixture	Cav (mm)	a (mm)	C/a	Crack type	K_{IC}, MPa.m$^{1/2}$
A	0.30	0.18	1.71	Palmqvist	1.95 ± 0.10
B	0.31	0.19	1.67	Palmqvist	1.80 ± 0.05
C	0.35	0.24	1.47	Palmqvist	1.50 ± 0.02
D	0.26	0.20	1.31	Palmqvist	2.30 ± 0.07

3. Results and discussion

3.1. Phase composition

Fig. 1 illustrates the XRD patterns of the four mixtures "A", "B", "C" and "D". The XRD pattern of the mixture "A" shows three phases; diopside, akermanite and olivine. The main crystalline phase was diopside ($CaO \cdot MgO \cdot 2SiO_2$: JCPDS #19-0239) with crystallite size of 130 nm, while akermanite ($Ca_2Mg\ (Si_2O_7)$: JCPDS#76-0841) with crystallite size of 102 nm and olivine (Mg_2SiO_4: JCPDS# 84-1402) with crystallite size of 80 nm were recorded as minor phases. New phase termed "baddeleyite" (ZrO_2: JCPDS # 13-0307) with crystallite size of 77 nm started to appear in mixture B. The appearance of this phase is attributed to the addition of ZrO_2. Along with the increase of ZrO_2, the amount of baddeleyite phase gradually increases at expense of other phases (diopside, akermanite and olivine). All mixtures A, B, C and D specimens sintered at 1325 ± 5 °C for 2 h.

3.2. 3.2. Microstructure

FESEM micrographs of the sintered specimens are illustrated in Fig. 2 (a-h). Low magnification micrographs of these composites, Fig. 2 (a, c, e and g), show a uniform distribution of pores and phases. High magnification images, Fig. 2 (b, d, f and h), reveals different colors; light white, grey and dark grey. Their EDX analysis indicated that the light white grains are zirconium oxide (baddeleyite) with two morphologies of zirconia grains: one is a small spherical shape and other is a large with irregular shape. The grey interface with sharp edges are diopside and dark grey color is olivine grains with a spherical shape. It's worth noting that the porosity level does not exceed 3% in all micrographs as a result of the optimum sintering temperature.

3.3. Physico-mechanical properties

The densification parameters in terms of bulk densities, apparent porosity and linear shrinkage of sintered specimens (A, B, C and D) are given in Table 5. It is obvious that there is no remarkable change in the porosity values of the investigated specimens where the apparent porosity values did not exceed 3%, while the bulk density was increased gradually by increasing ZrO_2 content from 0 to 25 wt.%. This change can be attributed to the formation of high density baddeleyite phase (5.75 g/cm^3) and the slight increase recorded in the shrinkage of mixture (A) to mixture (D) with increasing ZrO_2 content. This illustrates the reflection of the linear shrinkage on the density.

The mechanical parameters in terms of Vickers hardness and fracture toughness are recorded in Tables 6 and 7. As given in Tables, the obtained hardness value of the free zirconia specimen (A) is about 1.88 GPa, but the hardness of the specimens containing 5 and 15 wt.% of ZrO_2 were increased from 2.32 to 2.57 GPa, respectively. The further increase of zirconia up to 25 wt.%, the hardness of the specimen (D) was decreased to 2.25 GPa. In this context, hardness value recorded of specimens containing 5 wt.% of ZrO_2 (2.32 GPa) is considered the best and is higher than hardness of cortical and trabecular bone lamellae in the human femur (0.234 to 0.760 GPa) [29]. Therefore, this specimen can be proposed as implant materials. All sintered specimens with or without ZrO_2 revealed palmqvist crack which reflects the high fracture toughness values (K_{IC}) in particular the specimens containing 25 wt.% of ZrO_2. This is attributed to the presence of the high fracture toughness zirconia phase, which is characterized by martensitic transformation from monoclinic to tetragonal zirconia (m-$ZrO_2 \leftrightarrow$ t-ZrO_2) under cooling from sintering temperature to room temperature. Such kind of transformation generate cracks. These cracks are able to arrest the crack propagation and in turn improve the fracture toughness (K_{IC}) [30]. Table 8 gives the mechanical, physical and biological properties of all mixtures (A, B, C and D) and the most bioceramic materials which reported in the literature and cortical bone [31–42].

3.4. In-vitro bioactivity of the composites

Fig. 3 (a–h) shows the SEM micrographs and EDX analysis of the sintered specimens after soaking in simulated body fluid (SBF) for 7 days. Fig. 3 (a, c, e, g) clearly indicated that the hydroxyapatite was formed on the surface of all specimens. However, the amount of the hydroxyapatite precipitated on the surface of specimens changes from one specimen to another. This precipitate can be scattered, layered or multilayered but it depends on the amount. The whole surface of the sintered specimens containing 5 wt.% of ZrO_2 is completely covered with multilayered hydroxyapatite typical to cauliflower morphology. The surface of the sintered specimens containing 15 wt.% of ZrO_2 is covered with a single layer of hydroxyapatite. In contrast, scattered precipitate of HA was started to be appeared on the surface of the sintered free ZrO_2 specimen and the specimen containing 25 wt.% of ZrO_2. The formation of hydroxyapatite on surfaces of the specimens was confirmed by EDX analysis as seen in Fig. 3 (b, d, f, h). Ca/P atomic or molar ratio calculated from EDS is around 1.76. This ratio confirms the formation of HA. The scattered precipitate of apatite formation during 7 days on the surface of the sintered specimen (without zirconia) can be rationalized based on the akermanite phase because akermanite phase has good apatite mineralization and moderate dissolution and induces bone-like apatite formation after 5 days [43–47]. Interestingly, the bone-like apatite formation extremely increased with increasing zirconia content up to 15 wt.%. This result was not expected because the increase of zirconia content is accompanied by decreasing the content of the bioactive phase (akermanite). With the continuing increase of zirconia content

Table 8
The comparison of the properties of sintered specimens, the bioceramic materials most reported in the literature and cortical bone.

Material	Mixture (A)	Mixture (B)	Mixture (C)	Mixture (D)	Bredigite [31]	Wollastonite Coating [2]	HA Coating [2]	Akermanite [32]	HA [33,34]	γ-dicalcium silicate [35]	Diopside [33]	Cortical bone [29,36]
Hardness, GPa	1.88	2.32	2.57	2.25	–	2.50	1.20	–	6.00	3.62	–	0.234–0.760
Fracture Toughness, MPa · m$^{1/2}$	1.95	1.80	1.50	2.30	1.57	–	–	1.83	1.10	1.48	3.50	2.00–12.00
Density, g/cm^3	2.90	3.04	3.20	3.38	–	2.60	3.10	–	3.16	–	3.20	1.60–2.10
Porosity, %	3.50	2.30	2.30	2.96	–	5.30	7.00	–	–	–	–	–
Bioactivity	Slow	Very fast	Fast	Moderate	Fast	Moderate	Moderate	Moderate	Fast	Fast	Slow	–

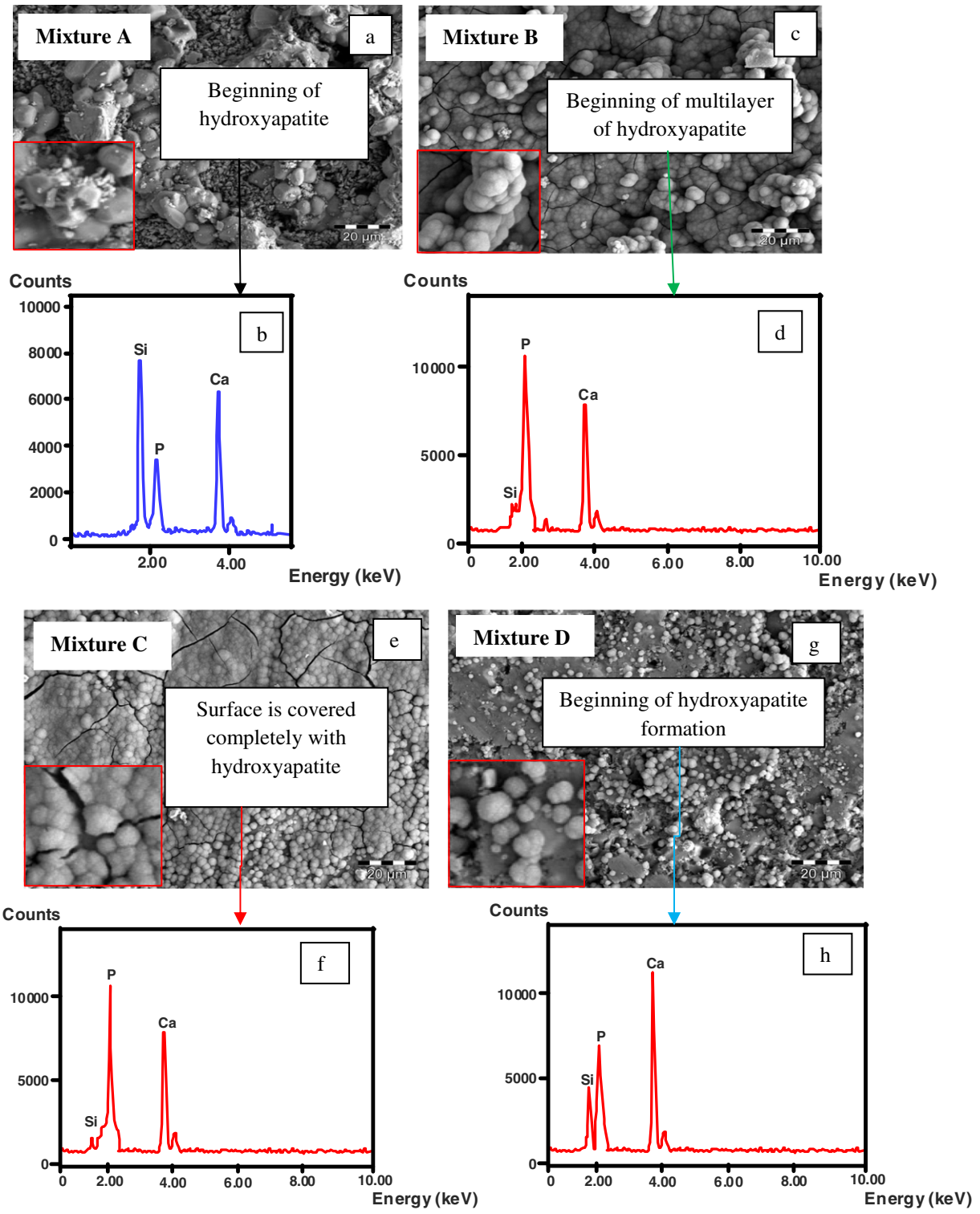

Fig. 3. SEM micrographs of the sintered A, B, C and D specimens after soaking in SBF for 7 days.

up to 25 wt.%, bone-like apatite formation was gradually decreased again. Bone-like apatite formation (bioactivity) greatly depends on phase composition and physical properties of the materials. Since the physical properties of all specimens are quite similar, the tendency of the specimens to form bone-like apatite based this factor must be excluded. The difference between specimens compositions are the content of zirconia at the expense of the phases developed during sintering such as akermanite, diopside and olivine, see XRD patterns of the specimens Fig. 1. In the view of the bioactivity, akermanite and its content were considered the effective element. Also, zirconia content (baddeleyite) and its reflection on the bioactivity of akermanite and vice versa was taken into consideration to understand the obtained data. The extreme formation of multi-layered bone-like apatite on the surface of the specimens containing 5 wt.% zirconia placed in SBF can be explained based on the reported data.

As previously investigated by Wu et al.[32,46], depletion of Ca, Mg and Si ions from akermanite phase into SBF starts to occur in the early stage (i.e. after one day) and their concentration increases with time.

This process is accompanied by the increase of pH as results of ion exchange of Ca cations in the akermanite ceramics with H cations in SBF. Consequently, a hydrated silica layer on the surface of the akermanite based ceramics and favorable sites for phosphate nucleation are formed. Accordingly, amorphous calcium phosphate with subsequent formation of bone-like apatite is formed by incorporating OH anions from SBF. This mechanism is favorable with our results but the content of bone-like apatite seems to be proportional to the content of akermanite phase. Another possible reaction mechanism is expected to be occurred and responsible about the formation of multi-layered bone-like apatite. Along with the little increase of the pH, hydroxylated zirconia surface (Zr-OH) is converted into negatively charged Zr—O bond. This in turns attracts Ca cations from SBF into the interface between the specimens and SBF then start to induce bone-like apatite nucleation in a similar manner as Si-OH [17,18]. In this context, it can be said that the amount of the akermanite phase in the specimen (B) is sufficient to give a reasonable concentration of Ca cations through ion exchange and increasing pH. This amount allows for the formation of bone-like apatite through ion exchange of Ca^{2+} ion from the depleted akermanite into the SBF solution with negatively charged surface (≡Si—O^- and Zr—O^-). With the increase of zirconia content to 15 wt.% at the expense of akermanite phase, the depleted amount of Ca^{2+} cations seems to be sufficient to increase the pH and in turns to activate the zirconia surface, therefore, the role of zirconia to induce bone-like apatite is acceptable but the formation of a single layer from apatite can be rationalized based on the amount of akermanite phase. The further increase of zirconia to 25 wt.% at the expense of akermanite phase, the depleted amount of Ca^{2+} cations is not sufficient to increase the pH and in turn the activation of the zirconia surface seems to be difficult, therefore, the role of zirconia to induce bone-like apatite is neglected and the formation of the apatite mainly depends on the amount of the akermanite.

3.5. Conclusions

The surface of the specimens containing 5 and 15 wt.% ZrO_2 were completely covered by hydroxyapatite layers (HA) typical to "cauliflower" morphology. Scattered precipitate of HA on the surfaces of ZrO_2 free specimens and the specimens containing 25 wt.% ZrO_2 was seen, but their surfaces did not completely cover. Vickers hardness and fracture toughness of the specimens of highly promised bioactivity (B & C) were 2.32–2.57 GPa and 1.8–1.5 MPa · $m^{1/2}$, respectively. The properties of these specimens are similar to the properties of human cortical bone as given in Table 8. Therefore, the specimen (B&C) mixtures are suited for bone implant materials.

References

[1] L.L. Hench, R.J. Splinter, W.C. Allen, T.K. Greenlee, Boding mechanism at the interface of ceramics prosthetic materials, J Biomed Mater Res Symp 2 (1971) 117–141.
[2] X.M. Liu, A. Carpi, B. Li, Bioactive calcium silicate ceramics and coatings, Biomed Pharmacother 62 (2008) 526–529.
[3] X. Liu, C. Ding, P.K. Chu, Mechanism of apatite formation on wollastonite coatings in simulated body fluids, Biomaterials 25 (2004) 1755–1761.
[4] P. Revell, E. Damien, X. Zhang, P. Evans, C. Howlett, The effect of magnesium ions on bone bonding to hydroxyapatite, Key Eng. Mater. 254-256 (2004) 447–450.
[5] H. Sun, C. Wu, K. Dai, J. Chang, T. Tang, Proliferation and osteoblastic differentiation of human bone narrow-derived stromal cells on akermanite-bioactive ceramics, Biomaterials 27 (2006) 5651–5657.
[6] C. Wu, J. Chang, Degradation, bioactivity and cytocompatibility of diopside akermanite and bredigite ceramics, J. Biomed. Mater. Res. B 83 (2007) 153–160.
[7] C. Wu, M. Zhang, D. Zhai, J. Yu, Y. Lui, H. Zhu, J. Chang, Containerless processing for preparation of akermanite bioceramic spheres with homogeneous structure, tailored bioactivity and degradation, J. Mater. Chem. B 1 (2013) 1019–1026.
[8] S. Ni, L. Chou, J. Chang, Preparation and characterization of frosterite (Mg_2SiO_4) bioceramics, Ceram. Int. 33 (2007) 83–88.
[9] M. Kharaziha, M.H. Fathi, Synthesis and characterization of bioactive forsterite nanopowder, Ceram. Int. 35 (2009) 2449–2454.
[10] M. Ferraries, H.E. Verne, P. Appendino, C. Moisescu, A. Rajewski, A. Ravaglioli, A. Piancastelli, Coatings on zirconia for medical applications, Biomaterials 21 (2001) 765–773.
[11] M. Bosetti, E. Verne, M. Ferraris, A. Ravaglioli, M. Cannas, In vitro characterisation of zirconia coated by bioactive glass, Biomaterials 22 (2001) 987–994.
[12] Y.W. Gua, A.U.J. Yapb, P. Cheanga, K.A. Khor, Effects of incroporation of HA/ZrO_2 into glass ionomer cement (GIC), Biomaterials 26 (2005) 713–720.
[13] H.W. Kim, S.Y. Lee, C.J. Bae, Y.J. Noh, H.E. Kim, H.M. Kim, J.S. Ko, Porous ZrO_2 bone scaffold coated with hydroxyapatite with flourapatite intermediate layer, Biomaterials 24 (2003) 3277–3284.
[14] V. Stanc, N.N. Aldini, M. Fini, G. Giavaresi, R. Giardino, A. Krajewski, A. Ravagliolie, M. Mazzocchie, B. Dubinia, M.G.P. Bossia, F. Rustichelli, Osteointegration of bioactive glass -coated zirconia in healthy bone: an in vivo evaluation, Biomaterials 23 (2002) 3833–3841.
[15] X.Y. Liu, C.X. Ding, Bioactivity of plasma sprayed wollastonite/ZrO_2 composite coating, Surf. Coat. Technol. 172 (2003) 270–278.
[16] S.F. Hulbert, The use of alumina and zirconia in surgical implants: in an introduction to bioceramics, in: L.L. Hench, J. Wilson (Eds.),World Scientific, Singapore 1993, pp. 25–40.
[17] M. Uchida, H.-M. Kim, T. Kokubo, Bonelike apatite formation induced on zirconia gel in a simulated body fluid and its modified solutions, J. Am. Ceram. Soc. 84 (9) (2001) 2041–2044.
[18] M. Uchida, H.-M. Kim, T. Kokubo, M. Nawa, T. Asano, K. Tanaka, T. Nakamura, Apatite forming ability of a zirconia alumina nano-composite induced by chemical treatment, J. Biomed. Mater. Res. 60 (2002) 277–282.
[19] T. Kokubo, H. Takadama, How useful is SBF in predicting in vivo bone bioactivity? Biomaterials 27 (2006) 2907–2915.
[20] ASTM C830-00, Standard Test Methods for Apparent Porosity, Liquid Absorption, Apparent Specific Gravity, and Bulk Density of Refractory Shapes by Vacuum Pressure. ASTM International, West Conshohocken, PA, Vol. 15, 2011.
[21] ASTM C1327-03, Test Method for Vickers Indentation Hardness of Advanced Ceramics. Annual Book of ASTM Standards, West Conshohocken, PA, Vol. 15, 2006.
[22] F. Sergejev, M. Antonov, Comparative study on indentation fracture toughness measurements of cemented carbides, Proc. Estonian Acad. Sci. Eng. 12 (2006) 388–398.
[23] K.K. Bamzai, P.N. Kotru, B.M. Wanklyn, Investigations on indentation induced hardness and fracture mechanism in flux grown $DyAlO_3$ crystals, Appl. Surf. Sci. 133 (1998) 195–204.
[24] H.J. Yount, Hardness and Fracture Toughness of Heat Treated Advanced Ceramic Materials for Use as Fuel Coating and Inert Matrix Materials in Advanced Reactors. M. Sc. University of Wisconsin Madison, 2006.
[25] H.R. Lawn, E.R. Fuller, Equilibrium penny-like cracks in indentation fracture, J. Mater. Sci. 10 (1975) 2016–2024.
[26] V. Keryvin, V.H. Hoang, J. Shen, Hardness, toughness, brittleness and cracking systems in an iron-based bulk metallic glass by indentation, Intermetallics 17 (2009) 211–217.
[27] L. Curkovic, V. Rede, K. Grilec, A. Mulabdic, Hardness and fracture toughness of alumina ceramics. 12 Th. Conference on materials, processes, friction and wear, Fac. Mech. Eng. Nav. Archit. (2007) Ivana Lucica 1, Zagreb, Croatia.
[28] M. Dietz, H.D. Tietz, Characterization of engineering ceramics by indentation methods, J. Mater. Sci. 25 (1990) 3731–3738.
[29] P.K. Zysset, X.E. Guo, C.E. Hoffler, K.E. Moore, S.A. Goldstein, Elastic modulus and hardness of cortical and trabecular bone lamellae measured by nanoindentation in the human femur, J. Biomech. 32 (1999) 1005–1012.
[30] B. Basu, Toughening of yttria-stabilised tetragonal zirconia ceramics, Int. Mater. Rev. 50 (2005) 239–256.
[31] C. Wu, J. Chang, J. Wang, S. Ni, W. Zhai, Preparation and characteristics of a calcium magnesium silicate (bredigite) bioactive ceramic, Biomaterials 26 (2005) 2925–2931.
[32] C. Wu, J. Chang, A novel akermanite bioceramic: preparation and characteristics, J. Biomater. Appl. 21 (2006) 119–129.
[33] T. Nonami, S. Tsutsumi, Study of diopside ceramics for biomaterials, J. Mater. Sci. Mater. Med. 10 (1999) 475–479.
[34] T.P. Hoepfner, E.D. Case, The influence of the microstructure on the hardness of sintered hydroxyapatite, Ceram. Int. 29 (2003) 699–706.
[35] Z. Gou, J. Chang, W. Zhai, Preparation and characterization of novel bioactive dicalcium silicate ceramics, J. Eur. Ceram. Soc. 1507–1514 (2005).
[36] L.L. Hench, Bioceramics: from concept to clinic, J. Amr. Ceram Soc. 74 (4) (1991) 1487–1510.
[37] P. Li, F. Zhang, The electrochemistry of a glass surface and its application to bioactive glass in solution, J. Non-Cryst. Solids 8 (1990) 112–119.
[38] V. Valet-Regi, A.J. Salinas, J. Roman, M. Gil, Effect of magnesium content on the in vitro bioactivity of CaO-MgO-SiO_2-P_2O_5 sol-gel glasses, J. Mater. Chem. 9 (1999) 515–518.
[39] L.L. Hench, Bioceramics, J. Am. Ceram. Soc. 81 (1998) 1705–17028.
[40] A. Ravaglioli, A. Krajewski, Bioceramics-Materials, Properties and Applications. London, Chapman &Hall, 1992.
[41] J.L. Shi, Thermodynamics and densification kinetics in solid-state sintering of ceramics, J. Mater. Res. 14 (4) (1999) 1398–1408.
[42] R.W. Rice, Grain size and porosity dependence of ceramic fracture energy and toughness at 22 °C, J. Mater. Sci. 31 (1996) 1969–1983.
[43] C. Wu, J. Chang, A review of bioactive silicate ceramics, Biomed. Mater. 8 (032001) (2013) 1–13.
[44] C.T. Wu, J. Chang, Synthesis and apatite-formation ability of akermanite, Mater. Lett. 58 (2004) 2415–2417.
[45] A.A. Nogiwa, D.A. Cortes, Bone-like apatite coating on Mg-PSZ/Al_2O_3 composites using bioactive systems, J. Mater. Sci. Mater. Med. 17 (2006) 1139–1144.
[46] C.T. Wu, J. Chang, S. Ni, J. Wang, In vitro bioactivity of akermanite ceramics, J. Biomed. Mater. Res. A 1 (2006) 73–80.
[47] E.M.M. Ewais, A. Moustafa, K. Pardun, K. Rezwan, Bioactivity investigations with calcia magnesia based composites, J. Mater. Sci. Eng. A5 (1–2) (2015) 21–36.